Article

Morphology Control of Hydroxyapatite as a Potential Reinforcement for Orthopedic Biomaterials: The Hydrothermal Process

Piotr Szterner *[ID], Agnieszka Antosik [ID], Joanna Pagacz [ID] and Paulina Tymowicz-Grzyb [ID]

Łukasiewicz Research Network, Institute of Ceramics and Building Materials, Cementowa 8,
31-983 Cracow, Poland; agnieszka.antosik@icimb.lukasiewicz.gov.pl (A.A.);
joanna.pagacz@icimb.lukasiewicz.gov.pl (J.P.); paulina.tymowicz@icimb.lukasiewicz.gov.pl (P.T.-G.)
* Correspondence: piotr.szterner@icimb.lukasiewicz.gov.pl

Abstract: Hydroxyapatite (HAp) of different morphologies was prepared by the direct decomposition of calcium lactate pentahydrate chelates using dipotassium hydrogen phosphate under hydrothermal conditions. The proposed technique allows for precise control of the HAp crystals morphology and product purity, which are necessary for biomedical applications. The synthesis parameters such as reagent concentrations, pH, reaction time, temperature, pressure, and stirring rate were optimized in order to produce calcium phosphates (CaPs) ceramics with restricted morphologies and composition. As a result, we obtained hydroxyapatite in the form of whiskers, hexagonal rods, nano particles, flowers, and cylinders. The products were characterized according to their structure (FTIR and XRD), morphology (SEM), and functional properties, i.e., the specific surface area. The obtained results indicate that the reagent concentration and pH values have the greatest impact on the HAp properties; however, the proper combination of all the mentioned parameters should be considered when there is a need for a bioceramic with defined physicochemical properties and an appropriate morphology.

Keywords: hydroxyapatite; whiskers; hexagonal rods; calcium lactate pentahydrate; hydrothermal synthesis; biomaterials

1. Introduction

In materials science, bioactive calcium phosphates (CaPs) ceramics have attracted great attention from researchers, mainly because of their biocompatibility and chemical and crystallographic similarities with the minerals in human hard tissues. Due to its unique physicochemical and biological properties, hydroxyapatite (HAp), ($Ca_{10}(PO_4)_6(OH)_2$), occupies a special place among calcium phosphates [1–4]. This biomaterial is one of the main components of human bones and teeth, and because of its excellent biocompatibility it is extensively used in implantology [5,6]. HAp is characterized by a high biotolerance and controlled resorption in the tissue environment, as well as an ability to create a permanent and strong connection with the surrounding bone tissue. Synthetic hydroxyapatite can be applied as a reinforcement for orthopedic biomaterials composed of polymers, thus providing better mechanical properties for the polymeric matrix. Regarding this aspect, synthetic HAp in a fibrous form is of particular importance compared to the currently available fibers [7–9].

The applications of hydroxyapatite are wide ranging, as it is used in various fields including technical and medical industries. Therefore, HAp can be utilized as a component of bone fillers and bone supplements, as well as an implant coating to facilitate osseointegration and osteointegration [10]. Moreover, HAp reduces dental caries in dental cements and pastes, toothpastes, and chewing gums [11–14], while in cosmetic products it can play the role of a tooth whitener, skin cleaner, or agent for hair dyes [15]. In pharmacology, hydroxyapatite nanoparticles can be useful for drug delivery [16–18] or as a system for controlled drug release [19]. From a technical point of view, HAp is used in chromatography [20],

catalysis [21], and systems for wastewater and soil treatment as an adsorbent of heavy metal ions [22,23]. Additionally, a photocatalytic effect of alumina/TiO_2/hydroxyapatite composites in air filters was found. These composites are efficient in absorbing and decomposing CO, and they are thus promising in terms of reducing automotive exhaust pollutants [24].

The chemical methods used for the production of HAp can be divided into two categories: dry methods involving solid phases, including reactions at high temperatures and pressures [25,26], and wet methods based on the precipitation of components from aqueous solutions. The dry methods group of synthesis techniques includes chemical precipitation [27], hydrolysis [28], sol–gel [29], hydrothermal [30,31], emulsion [32], and sonochemical methods [33,34]. With an aim of controlling the process of ceramic formation, the hydrothermal processing method seems to be the perfect solution. During this procedure, the hydroxyapatite is precipitated from an overheated solution, which allows researchers to regulate of the rate and uniformity of crystallization. As a result, it is possible to produce ceramics with a specified size and morphology [35].

The influence of different conditions of hydrothermal synthesis, such as temperature or pH on the HAp morphology has been the subject of various studies [36–43]; however, none of them have dealt with the synthesis procedure presented in this paper. Liu et al. [36] showed the influence of time and pH on the hydrothermal reaction of $Ca(OH)_2$ and $CaHPO_4 \cdot 2H_2O$. Different conditions of pH = 6–14 and temperature in the range of 60–140 °C have been tested, and the authors concluded that pH value is an important parameter influencing the HAp morphology.
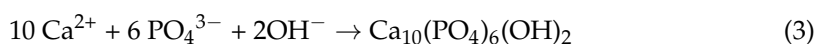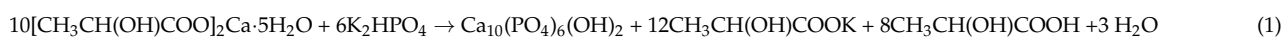
The effects of time, temperature, and pH on the reaction of $Ca(NO_3)_2 \cdot 4H_2O$ with $(NH_4)_2HPO_4$ under hydrothermal conditions were investigated by Ebrahimi et al. [37]. The authors presented the influence of pH values on the crystallinity, particle size, and yield of HAp. They observed that the yield of a reaction increased in alkaline conditions and pH strongly affected the size and crystallinity of HAp. Similar studies on the morphology of HAp obtained by a hydrothermal reaction of $Ca(OH)_2$ and $Ca(NO_3)_2 \cdot 4H_2O$ were reported by Ortiz et al. [38]. The authors showed an important effect of H^+ on the morphological and crystallographic characteristics of HAp. Their results proved that the nanoparticles' appearance and phase composition change depending on the pH, and they also showed a strong relation with the amount of H+ and OH- ions. Suchanek et al. studied the influence of pH on the structural and morphological evolution of CaPs particles [39]. The authors found that the kind of synthesized calcium phosphates strongly depends on the pH. In accordance with the solubility phase diagram for CaPs, at a pH lower than 4.2, the least soluble (i.e., most stable) compound is monetite (dibasic calcium phosphate anhydrous, DCPA), while for pH values higher than 4.2, HAp is the most thermodynamically stable phase. On the other hand, Kati et al. [40] presented a report on the effects of reaction time and heat treatment of hydroxyapatite obtained during the reaction of $Ca(NO_3)_2 \cdot 4H_2O$ and P_2O_5 in the hydrothermal process. The authors noted that as the synthesis time increased, more agglomerates appeared. Additionally, Kuśnieruk et al. [41] found that for the reaction between $Ca(OH)_2$ and H_3PO_4, the average HAp size can be controlled by the proper choice of synthesis conditions such as time, temperature, and pressure. The effects of the initial Ca^{2+} ion concentration, pH, and Ca/P ratio on the structural characteristic and morphology of HAp whiskers were investigated by Zhang et al. [42] for a reaction between $Ca(OH)_2$ and H_3PO_4. The authors noticed that at a low pH and with low Ca/P values, branch-like whiskers and irregular plate-like particles were synthesized, while high pH values favored the creation of lath-like hydroxyapatite at high Ca/P ratio.

A complex study by Roeder et al. included the effects of the heating rate, stirring rate, and temperature of the process for the reactions of DL-lactic acid ($C_3H_6O_3$), $Ca(OH)_2$, and H_3PO_4. The authors observed that the temperature and reaction heating rate had only a comparably minor effect on the width of HAp whiskers [43].

The presented work is a part of our extensive research on the use of calcium lactate pentahydrate and different phosphate precursors for the hydrothermal synthesis of hydrox-

yapatite. It should be emphasized that the choice of this synthesis technique is because of the possibility of controlling the HAp crystal morphology and resulting product purity, which are the most important requirements for biomedical applications. In our previous works [44,45] we investigated HAp fabrication using calcium lactate pentahydrate and orthophosphoric acid and the effects of the process parameters such as reaction time and temperature on HAp morphology and phase composition.

In this work, we followed another procedure for HAp synthesis, which is a direct reaction between calcium lactate pentahydrate and dipotassium hydrogen phosphate. We planned, as before, to examine the effects of different factors on HAp characteristics, such as reagent concentrations, pH, reaction time and temperature, pressure, and stirring rate. The general reaction during the hydrothermal synthesis of hydroxyapatite from calcium lactate pentahydrate and dipotassium hydrogen phosphate is presented below (reaction 1). The synthesis is based on the thermal decomposition of calcium chelates in specific conditions (high temperature up to 200 °C and high pressure up to 20 bar). In the first step of the process calcium ions Ca^{2+} are formed (reaction 2), which next react with the phosphate groups (PO_4^{3-}) and hydroxyl groups (OH^-) (reaction 3) [43,44,46], as is shown below:

$$10[CH_3CH(OH)COO]_2Ca \cdot 5H_2O + 6K_2HPO_4 \rightarrow Ca_{10}(PO_4)_6(OH)_2 + 12CH_3CH(OH)COOK + 8CH_3CH(OH)COOH + 3\,H_2O \tag{1}$$

$$[CH_3CH(OH)COO]_2Ca \cdot 5H_2O \rightarrow Ca^{2+} + 2CH_3CH(OH)COO^- + 5H^+ + 5OH^- \tag{2}$$

$$10\,Ca^{2+} + 6\,PO_4^{3-} + 2OH^- \rightarrow Ca_{10}(PO_4)_6(OH)_2 \tag{3}$$

To the best of our knowledge, no data about hydrothermal synthesis with the direct use of calcium lactate pentahydrate and dipotassium hydrogen phosphate have been published, nor data about the exploration of the effect of reaction conditions on hydroxyapatite morphology and its phase composition. Regarding potential HAp application in the biomedical field, it is of particular importance to produce material with the desired structure, the possibility of chemical modification, and durability. In the case of apatites, for example nanosized HAp particles, they are characterized by high specific surface area which facilitates modification, while bigger whisker-shaped particles offer structural reinforcement in polymeric biocomposites. Thus, our goal was to study possibilities for HAp production with different morphologies for use in the biomedical field. The ceramics obtained in our study were described using the following techniques: scanning electron microscope (SEM), scanning transmission electron microscopy (STEM), X-ray diffraction method (XRD), Fourier transform infrared spectroscopy (FTIR), and Brunauer–Emmett–Teller (BET) surface area analysis. The crystal lattice parameters were determined in order to check the occurrence of differences in hydroxyapatite with different morphology. The obtained results allow the identification of optimal reaction parameters, which enable obtaining Hap with a specific morphology.

2. Materials and Methods

2.1. Materials

The synthesis was carried out using the following substrates: calcium lactate pentahydrate $C_6H_{10}CaO_6 \cdot 5H_2O$ (pure p.a., CAS: 5743-47-5) and dipotassium hydrogen phosphate K_2HPO_4 (pure p.a., CAS: 7758-11-4) from Chempur® Chemical Company, Poland. All materials were of analytical grade and used without any additional purification procedures.

2.2. Synthesis of HAp

HAp was fabricated using the hydrothermal method, similar to our previous studies [44,45]. Syntheses were carried out in various conditions using a stainless steel reactor (Büchiglasuster®, miniclave steel type 3/300 mL, 100 bar, Büchi AG, Uster, Switzerland).

For all syntheses, the concentration of Ca^{2+} ion was in the range of 0.025 to 0.2 mol/dm³, and the Ca/P molar ratio in the reaction mixture was 1.67, which is equivalent to that of stoichiometric HAp. The calcium lactate pentahydrate was dissolved in deionized water

and then dipotassium hydrogen phosphate was added. When a homogenous mixture was obtained, nitric acid was added to avoid the precipitation of calcium phosphate. The prepared reaction mixture was poured into a reaction vessel and during hydrothermal synthesis, the temperature and pressure inside the reactor were continuously monitored. The reactor with the heating assembly was placed on the magnetic stirrer (IKA®, RH basic, Staufen, Germany) with a heating temperature ranging between 50 and 320 °C and a speed ranging from 100 to 2000 rpm. Upon completion of each reaction, the vessel was cooled to ambient temperature (∼25 °C) overnight. The product was then filtered off, washed quickly with deionized water four times, and finally dried in the air in the laboratory dryer (KCW-100, PREMED, Marki, Poland) at 100 °C for at least 20 h. Reaction conditions were controlled by a heating assembly (800W, Termtech, Warsaw, Poland Bristol, UK), temperature controller (RE72, LUMEL), thermocouple (TP-234k-b-200, Czaki® Thermo-Product, RASZYN-Rybie, Poland), and the installed manometer. All parameters of the heating process (e.g., temperature and heating time) were additionally controlled by Program Lumel Process 1.2 (Lumel S.A, Zielona Góra, Poland). The pH of the solution at start and end of the reaction was measured with a glass pH electrode (Eutech Instruments, Singapore, CyberScan PCD 6500) at 25 °C.

During the reaction, the effect of parameters such as: (a) Ca^{2+} ions concentration (0.025–0.2 mol/dm^3), (b) time of reaction (1, 3, and 5 h), (c) temperature (110–200 °C) and pressure of reaction (2–20 bar), (d) stirring rate, and (e) pH of mixture reaction (3.48–11.01) was investigated.

2.3. Characterization

2.3.1. Morphology and Compositional Analysis

To define the microstructure (shape and grain size) of the CaPs ceramics, scanning electron microscopy with field emission was applied (Nova NanoSEM 200, FEI, Brno, Czech Republic). Samples were mounted on aluminum stubs using carbon double-sided adhesive tape, those in nanometric sizes were additionally coated using a plasma coater (EM SCD500, Leica) that applied 25 nm of gold film. The SEM observations were performed in low vacuum conditions using backscattered electrons at 15 kV accelerating voltage (to observe elongated and fibrous particles) or in high vacuum conditions using secondary electrons detector (to observe nanometer particles) at 18.5 kV accelerating voltage.

Additionally, the scanning electron microscope was retrofitted by adding a two-segment solid-state STEM detector to allow for transmission observations. Powder samples were placed on copper grids with carbon films and were observed at 15 and 20 kV accelerating voltage.

2.3.2. X-ray Diffraction Method (XRD)

The phase composition of synthesized powders was characterized by powder X-ray diffraction (XRD) (D8 Advance, Bruker-AXS, Karlsruhe, Germany) in the Bragg–Brentano geometry. Measurements were carried out at 2θ from 5 to 120° at a step width of 0.01° and rate of 2 s/step under ambient conditions using Cu-Ka (λ = 0.154 nm) as a radiation source at a current of 40 mA with a voltage of 40 kV. The obtained XRD patterns were identified with reference to the Crystallography Open Database (COD) using DIFFRACplus EVA-SEARCH software. The quantity of each phase was calculated by the Rietveld method using "DiffracPlus Topas" software. Before X-ray analysis, all HAp samples were lightly ground manually with a mortar and pestle.

2.3.3. Fourier Transform Infrared Spectroscopy (FTIR Analysis)

The infrared spectra were recorded on a Bruker TENSOR 27 instrument equipped with a DLaTGS detector. Powder samples were analyzed in the transmission mode with the following instrumental settings: wavenumber range 400–4000 cm^{-1}, number of scans 64, and spectral resolution 4 cm^{-1}. Each sample was measured twice to check the repeata-

bility. The baseline correction procedure was applied to the presented spectra with Opus 7.2 software.

2.3.4. Brunauer–Emmett–Teller (BET) Surface Area Analysis

The specific surface area of samples was determined with the BET method using Gemini VII 2390t Micromeritics instrument (Norcross, GA, USA). The nine-point nitrogen adsorption and desorption isotherm were registered in the pressure range of 0.05–0.25 p/p°, where p and p° are the equilibrium and the saturation pressure of adsorbates at the temperature of adsorption, respectively. The measurements were performed at the temperature of liquid nitrogen. Before the measurement, samples were degassed at 105 °C in nitrogen atmosphere for 1 h in order to dry and purify the investigated materials.

3. Results

Depending on the hydrothermal process parameters, products with different phase compositions and different morphologies can be obtained. In this section, we present the results of systematic studies on the hydrothermal process in relation to reagent concentration, time and temperature of the process, pH, and the stirring rate. Optimal conditions for the synthesis were identified.

3.1. Identification of the Optimum Ca^{2+} Ions Concentration and Time of Reaction

Aiming at identification of the optimum Ca^{2+} ions concentration and time of reaction, the effect of these two parameters on the morphology and phase composition of HAp was determined for the process carried out at 200 °C under a pressure of 20 bar and stirring rate of 250 rpm. The pH of the starting solution oscillated around values of 4. The variable factors were as follows: Ca^{2+} concentration was 0.025 mol/dm^3, 0.05 mol/dm^3, 0.1 mol/dm^3, 0.15 mol/dm^3, and 0.2 mol/dm^3; the reaction time was 1 h, 3 h, and 5 h for each Ca^{2+} concentration (Table 1).

Table 1. The effect of Ca^{2+} concentration and reaction time on the morphology and phase composition of the obtained products (reaction temperature 200 °C, pressure 20 bar, stirring rate of 250 rpm, and the reaction heating rate of 2.5 °C/min).

Ca^{2+} mol/dm^3	pH before Synthesis	Time h	Length μm	Width μm	Phase Composition (Form)
0.025	3.65		14.44–54.54	1.11–4.44	HAp (whiskers)
0.05	3.99		6.18–56.82	0.66–1.72	HAp (whiskers)
0.1	3.61	1	6.82–27.27	0.91–2.77	HAp (hexagonal rods)
0.15	3.27		11.11–52.22	1.11–4.0	HAp (hexagonal rods)
0.2	3.22		12.72–57.77	0.45–1.55	92.35% HAp (hexagonal rods), 7.65% Monetite (plate formations)
0.025	4.40		5.45–66.67	0.44–2.44	HAp (whiskers)
0.05	4.01		11.11–88.89	0.91–1.82	HAp (whiskers)
0.1	3.20	3	12.22–55.55	0.44–1.55	HAp (hexagonal rods)
0.15	3.56		4.54–33.33	0.91–3.2	HAp (hexagonal rods)
0.2	3.38		5.91–27.27	0.66–2.72	HAp (hexagonal rods)
0.025	4.11		10.0–77.27	0.91–1.82	HAp (whiskers)
0.05	4.53		4.54–44.44	0.44–1.11	HAp (whiskers)
0.1	3.65	5	4.54–22.72	0.45–1.82	HAp (hexagonal rods)
0.15	3.44		5.91–27.27	0.91–2.27	HAp (hexagonal rods)
0.2	3.24		5.33–21.11	0.44–1.33	HAp (hexagonal rods)

In this part of the study, we used SEM, XRD, and IR spectroscopy to identify the differences between the obtained HAp ceramics, as well as the physical adsorption method to follow changes in the specific surface area.

The comparison of SEM images of products obtained during 5 h of synthesis at different Ca^{2+} concentrations is shown in Figure 1.
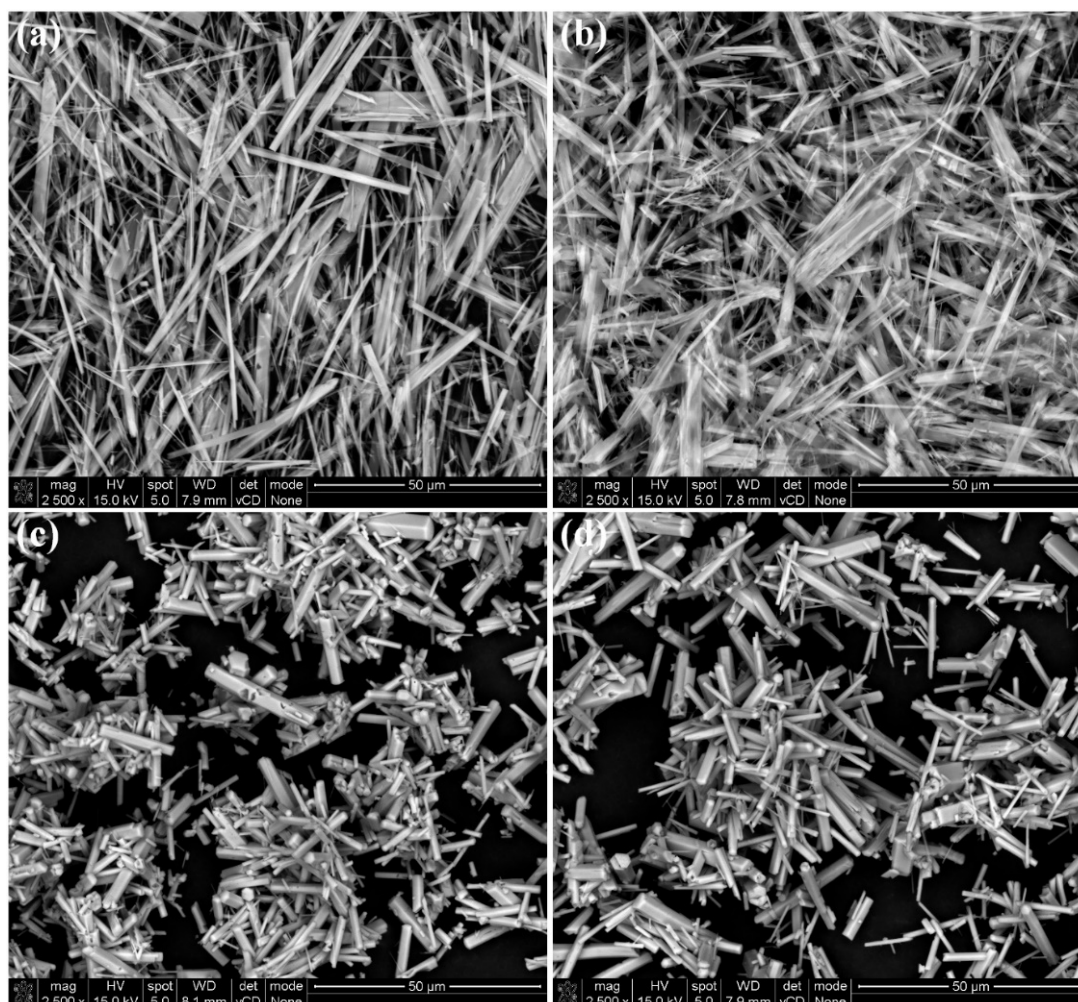

Figure 1. SEM images of products obtained in hydrothermal synthesis (200 °C, 20 bar, and 5 h) for different Ca^{2+} concentrations: (**a**) 0.025 mol/dm^3, (**b**) 0.05 mol/dm^3, (**c**) 0.15 mol/dm^3, and (**d**) 0.2 mol/dm^3 (magnification of 2500×).

The observed influence of calcium ions concentration on the HAp's appearance was the same for all reactions carried out at 200 °C, 20 bars, and reaction time 1–5 h. Two different morphological forms were identified. The products in the form of whiskers were obtained for Ca^{2+} ion concentration of up to 0.05 mol/dm^3, while for Ca^{2+} ion concentration of more than 0.1 mol/dm^3, hexagonal rods were observed (Table 1, Figure 1).

The Ca^{2+} ion concentration also affected the dimensions of the particles. As the concentration increases, the length of the whiskers or rods decreases. The mean length of the whiskers prepared in a time of 5 h at Ca^{2+} ion concentrations up to 0.05 mol/dm^3 (4–77 μm) was higher than the length of hexagonal rods prepared at Ca^{2+} ion concentration of 0.1–0.2 mol/dm^3 (4.5–21.1 μm).

The SEM images of products obtained during the different times (1, 3, and 5 h) and with Ca^{2+} ion concentrations of 0.025 mol/dm^3 and 0.2 mol/dm^3 are presented in Figure 2. Therefore, the influence of the reaction time can be estimated.
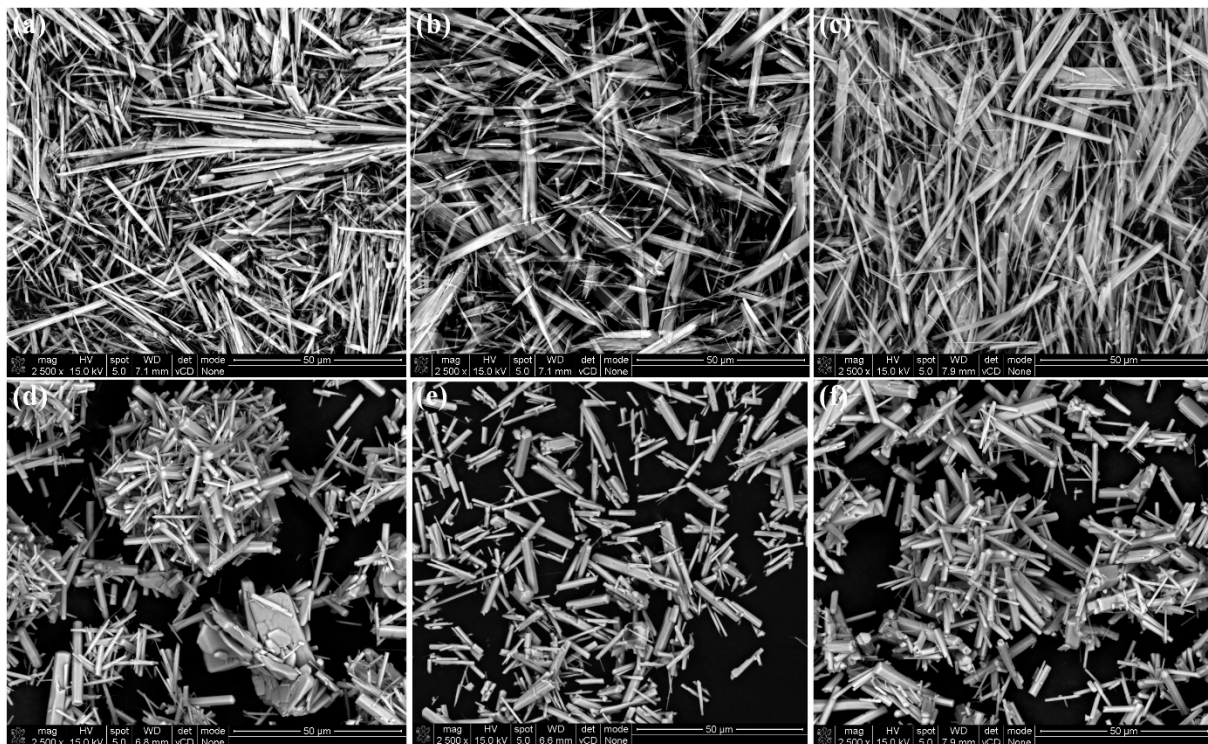
Figure 2. SEM images of products obtained in hydrothermal synthesis (200 °C, 20 bar) for whiskers at Ca^{2+} 0.025 mol/dm^3: (**a**) 1 h, (**b**) 3 h, and (**c**) 5 h. Additionally, for hexagonal rods at Ca^{2+} 0.2 mol/dm^3: (**d**) 1 h, (**e**) 3 h, and (**f**) 5 h (magnification of 2500×).

As shown in Table 1 and Figure 2, the reaction with a Ca^{2+} ion concentration of 0.025 mol/dm^3 led to products in the shape of whiskers regardless of the reaction time, which only influenced the length of the obtained particles (increase), whereas for the reaction conducted with a Ca^{2+} ion concentration of 0.2 mol/dm^3, the reaction products were formed as hexagonal rods. In contrast to the above results, in this case, as the reaction time increases, the length of the obtained particles decreases. Additional study with STEM device for materials obtained during 5 h of synthesis (Figure S1, Supplementary materials) resulted in the observation that both whiskers and hexagonal rods have a smooth surface and clear contours.

Figure 3 presents the XRD patterns of HAp synthesized at different Ca^{2+} ion concentrations (200 °C and 5 h). According to the phase analysis, the patterns of all powders are nearly the same and typical for pure hydroxyapatite (hexagonal and P 63/m space group). The database card number (COD) of the compounds used to identify the phase composition in the samples are listed in Table 2. The shape of the diffraction patterns indicates a high degree of crystallinity in the materials under study. A slight increase in an intensity of the peak (300) at 2θ = 32.9° in the sample with 0.025 Ca^{2+} probably is caused by the texturing of long whisker particle samples. The synthesized hydroxyapatite is mainly oriented along the *c*-axis direction of the hexagonal crystal structure [47].
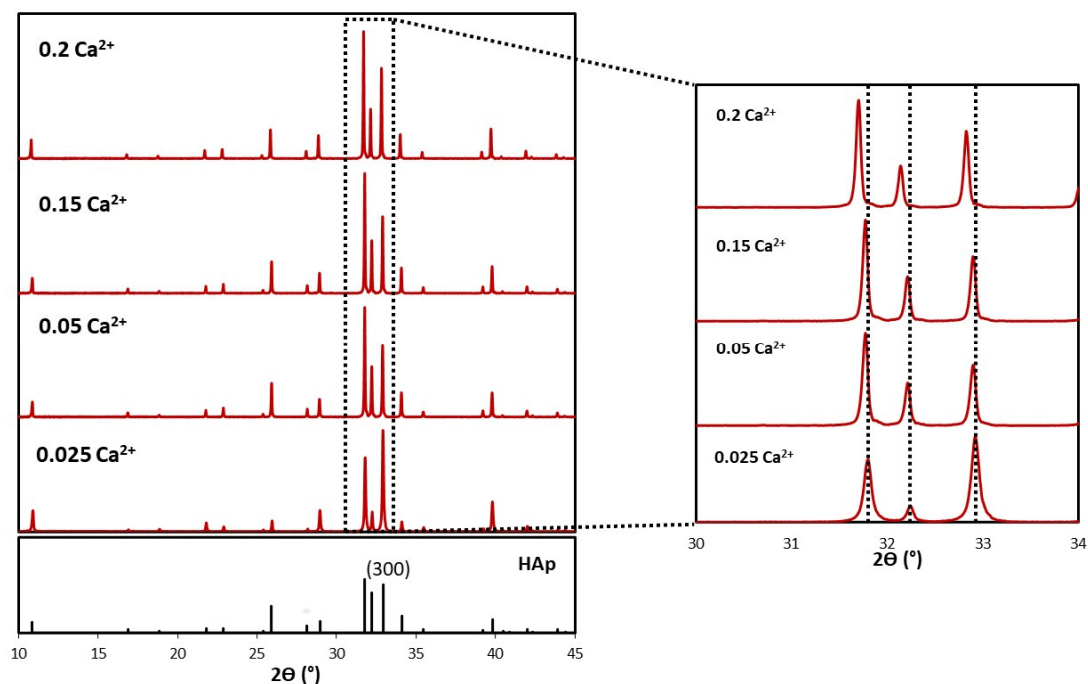
Figure 3. XRD patterns of synthesized HAp powders obtained in hydrothermal synthesis (200 °C, 20 bar, 250 rpm, and 5 h) at different Ca^{2+} ion concentrations.

Table 2. Effect of Ca^{2+} ion concentration on the lattice parameters of the phases in the synthesized ceramic powders (for all samples: reaction conditions 200 °C, 20 bar, 250 rpm, and 5 h).

Ca^{+2} Ion Concentration mol/dm³	Phase Composition	COD	Crystal Lattice Parameters		
			$a = b$ (Å)	c (Å)	V * (Å³)
0.025	HAp	9001233 [48]	9.41660	6.87450	527.91
0.05	HAp	9011092 [49]	9.42400	6.87900	529.09
0.15	HAp	9011092 [49]	9.42400	6.87900	529.09
0.2	HAp	9002214 [50]	9.43940	6.88610	531.36

* cell volume.

Figure 4 shows the XRD patterns of powders with 0.025 and 0.2 mol/dm³ Ca^{2+} ion concentrations obtained with different reaction times and at the temperature of 200 °C. The database card numbers (COD) of the compounds used to identify samples as well as lattice parameters of the present phases are listed in Table 3. The measurements showed that in the case of powder with 0.025 mol/dm³ the Ca^{2+} ion concentrations, the reaction time did not significantly affect the phase composition and the crystal structure of samples. All powders represent XRD patterns characteristic for hydroxyapatite (hexagonal and P 63/m) with a strong tendency to the orientation of crystallites. A more noticeable effect of the reaction time on the phase composition was observed when the Ca^{2+} ion concentration was 0.2. In this case, after 1 h of reaction, the major component was hydroxyapatite (92.35%) and the small peaks corresponding to the monetite phase (DCPA, triclinic, P-1, 7.65%) were visible. The extension of the reaction time allowed us to obtain pure hydroxyapatite (hexagonal and P 63/m). Additionally, with an increase in the reaction time, the XRD patterns shifted to lower 2θ values. The *a* and *c* parameters increased; therefore, cell volume also increased, which may indicate the formation of hydroxyapatite with carbonate groups.
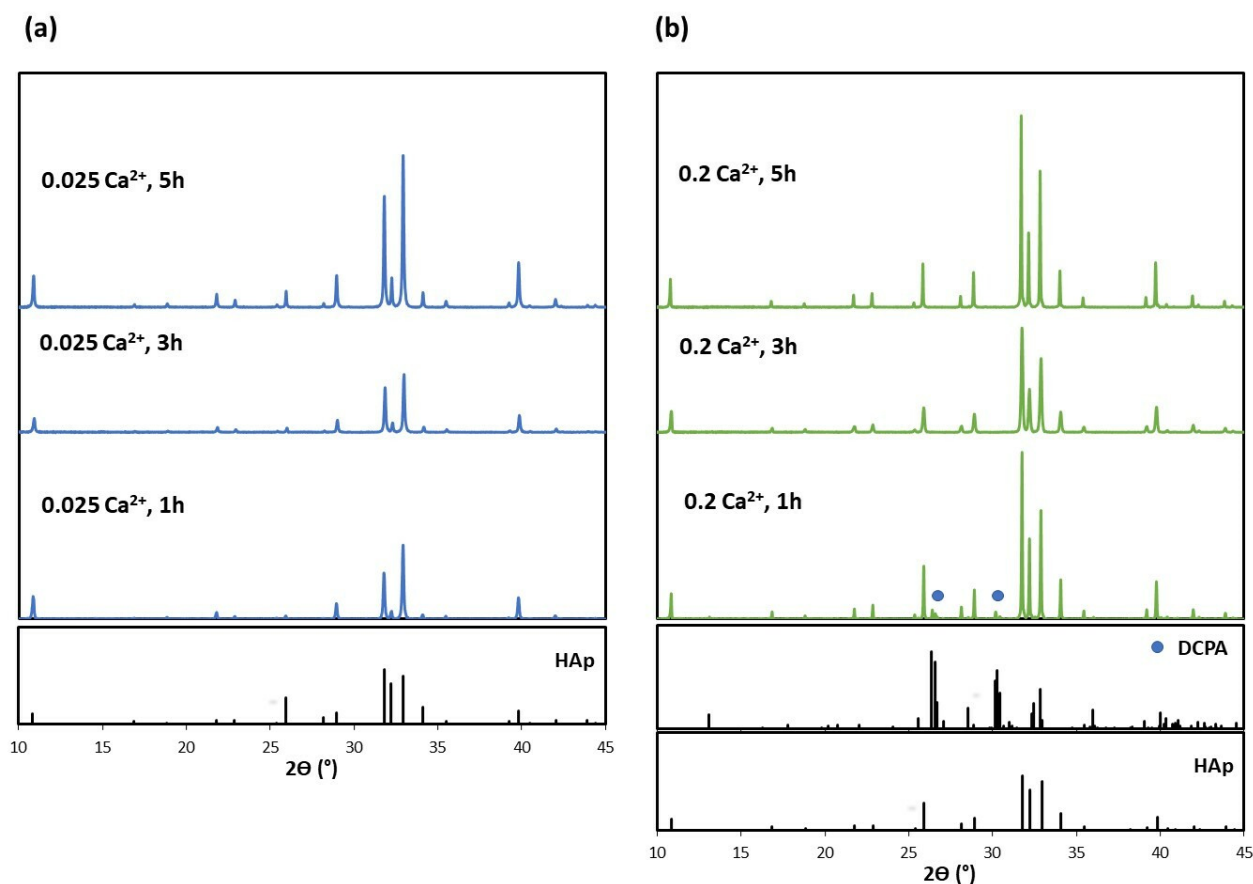
(a)

(b)

Figure 4. XRD patterns of powders with (**a**) 0.025 and (**b**) 0.2 mol/dm^3 Ca^{2+} ion concentrations obtained with different reaction times and at a temperature of 200 °C.

Table 3. Effect of the reaction time on the lattice parameters of the phases present in the synthesized powders at 200°C.

Ca^{2+} Ion Concentration mol/dm^3	Time	Phase Composition	COD	Crystal Lattice Parameters			
				a (Å)	*b* (Å)	*c* (Å)	*V* * (Å^3)
0.025	1 h	HAp	9001233 [48]	9.41660	9.41660	6.87450	527.91
	3 h	HAp	9001233 [48]	9.41660	9.41660	6.87450	527.91
	5 h	HAp	9001233 [48]	9.41660	9.41660	6.87450	527.91
0.2	1 h	HAp	9011092 [49]	9.42400	9.42400	6.87900	529.09
		DCPA	9007619 [51]	6.91000	6.62700	6.99800	309.28
	3 h	HAp	9011092 [49]	9.42400	9.42400	6.87900	529.09
	5 h	HAp	9002214 [50]	9.43940	9.43940	6.88610	531.36

* cell volume.

The FTIR spectra of materials obtained during 5 h hydrothermal synthesis carried out at 200 °C and different Ca^{2+} concentrations of (a) 0.025 mol/dm^3, (b) 0.05 mol/dm^3, (c) 0.1 mol/dm^3, (d) 0.15 mol/dm^3, and (e) 0.2 mol/dm^3 are shown in Figure 5.
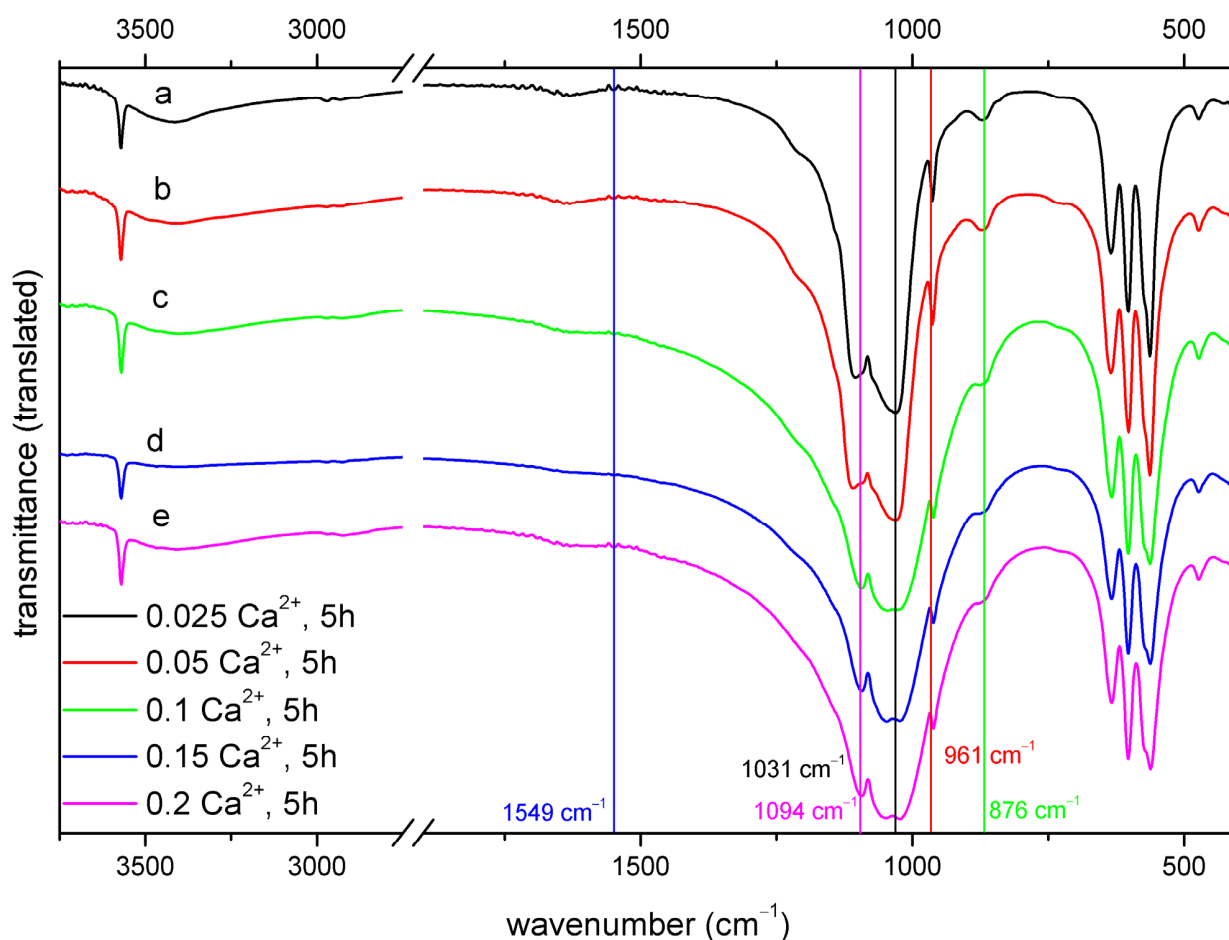
Figure 5. IR spectra of materials obtained from the solution with the Ca^{2+} concentration of (a) 0.025 mol/dm^3, (b) 0.05 mol/dm^3, (c) 0.1 mol/dm^3, (d) 0.15 mol/dm^3, and (e) 0.2 mol/dm^3 (5 h and 200 °C).

The identified IR bands assignments for the hydroxyapatites under investigation are presented in Table S1 [52,53]. The materials showed almost all characteristic bands for hydroxyapatite [54]. The sharp band at about 3571 cm^{-1} is related to the vibrations of hydroxyl groups on the HAp surface, while the bands observed around 3415 cm^{-1} and 1631 cm^{-1} proved the presence of water in the structure. Medium bands in the range of 872–878 cm^{-1}, assigned to ν_3 C-O (CO_3^{2-}) vibrations, are a singular proof of the carbonate ion's presence in the obtained ceramics. The other bands related to CO_3^{2-} around 1462 cm^{-1} are fairly visible. The four vibrational modes of phosphate ions were also identified at ν_1 962 cm^{-1}, ν_2 473 cm^{-1}, ν_3 1092 + 1031 cm^{-1}, and ν_4 603 + 562 cm^{-1}. The band at about 634 cm^{-1} can be assigned to both the O-H and labile PO_4^{3-} [55]. The shoulder observed at around 1210 cm^{-1} for almost all materials—except of those obtained at 0.15 and 0.2 Ca^{2+} concentration—can be assigned to the stretching vibration of P = O. A very weak band at around 427 cm^{-1} is probably due to impurities in $H_2PO_4^-$ or $P_2O_7^{4-}$.

When comparing the resulting IR spectra, the following observations can be formulated:

(a) The band at 867 cm^{-1} is the most intensive for the material Ca^{2+} 0.05 and 1 h;

(b) A change in the band at 872 cm^{-1}—for samples with Ca^{2+} ion concentrations of 0.1, 0.15, and 0.2 mol/dm^3—is less clear and shifted to the higher wavenumber of 876 cm^{-1};

(c) In samples with Ca^{2+} ion concentrations of 0.025 and 0.05 mol/dm^3, both the 1105 cm^{-1} and 1090 cm^{-1} bands are visible, while for the rest of the tested materials only one signal around 1092 cm^{-1} was identified;

(d) The split of the band at 1031 cm^{-1} was observed for materials with Ca^{2+} ion concentrations of 0.025 and 0.05 mol/dm^3 and for two bands in samples with Ca^{2+} ion concentrations of 0.1, 0.15, and 0.2 mol/dm^3;

(e) The bands at 1143 cm^{-1} and 1207 cm^{-1} are visible for the sample with Ca^{2+} ion concentration of 0.025 mol/dm^3; for the rest of the tested materials the bands are less visible or were not identified at all;

(f) Higher intensity of the band at 962 cm^{-1} for the materials with Ca^{2+} ion concentrations of 0.025 and 0.05 mol/dm^3;

(g) Slight changes in the bands related to OH groups in the range of 3400–300 cm^{-1}. For samples with Ca^{2+} ion concentrations 0.1, 0.15, and 0.2 mol/dm^3, an additional band at around 3468 cm^{-1} is present.

Below, the IR spectra for materials with different Ca^{2+} ion concentrations and the same time of the reaction (1 h) were presented (Figure 6). It was observed that the band related to OH groups is broader for material with Ca^{2+} 0.05 mol/dm^3. Moreover, the band at 1206 cm^{-1} in material with Ca^{2+} 0.2 mol/dm^3 disappeared. Similar to the above results, a split of the signal at 1031 cm^{-1} for two bands at 1048/1026 cm^{-1}, was observed, and the band at 963 cm^{-1} related to P-O stretching vibration is of lower intensity for materials with Ca^{2+} 0.2 mol/dm^3, like in the case of a band corresponding to carbonate ions at around 876 cm^{-1}.
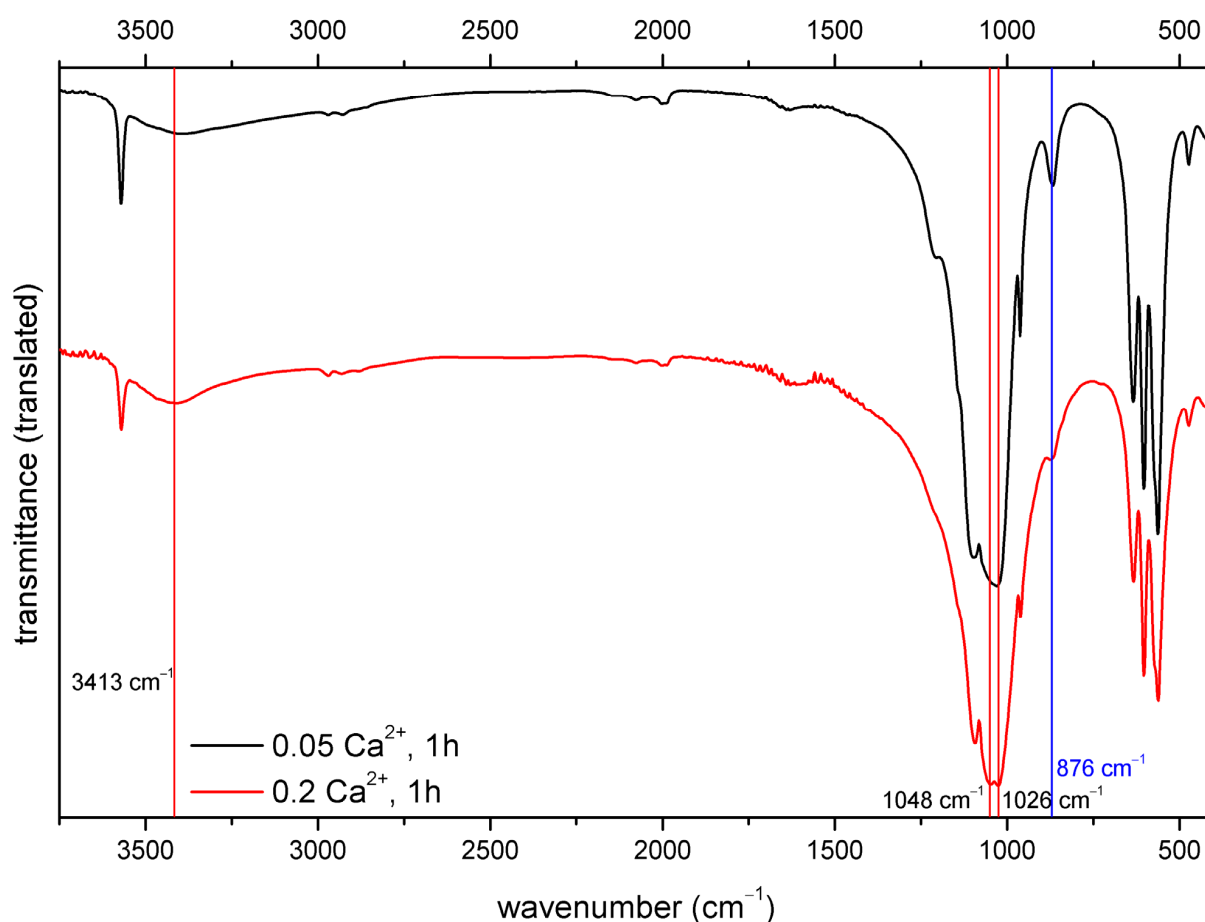

Figure 6. IR spectra of materials prepared with Ca^{2+} concentration of 0.05 mol/dm^3 and 0.2 mol/dm^3 (1 h and 200 °C).

The specific surface area was determined by the Brunauer–Emmett–Teller (BET) method [56]. The adsorption of gases in multimolecular layers Brunauer–Emmett–Teller (BET) theory aims to explain the physical adsorption of gas molecules on a solid surface

and is the basic analytical technique for the determination of the specific surface area of materials [57]. For synthesized hydroxyapatite of different morphologies and prepared during a 5 h reaction at a temperature of 200 °C, the specific surface area (S_{BET}) was obtained.

S_{BET} decreased with increasing concentration of Ca^{2+}, due to the grain growth of HAp:

- Whiskers obtained at Ca^{2+} of 0.05 mol/dm^3 S_{BET} was 6.6538 ± 0.0503 m^2/g;
- Hexagonal rods obtained at Ca^{2+} of 0.2 mol/dm^3 S_{BET} was 0.9310 ± 0.0146 m^2/g;
- Nano rods obtained at Ca^{2+} = 0.05 mol/dm^3 S_{BET} was 71.3623 ± 0.2185 m^2/g.

Based on these obtained results, it is possible to identify the optimal concentration of calcium and reaction time to obtain pure hydroxyapatite with the desired morphology. The optimal conditions for obtaining whiskers are a Ca^{2+} ion concentration of 0.05 mol/dm^3 and a reaction time of 5 h, whereas the optimal conditions for obtaining hexagonal rods are a Ca^{2+} ion concentration of 0.2 mol/dm^3 and a reaction time 5 h. A shorter reaction time results in the formation of monetite, which is an intermediate product during the reaction.

3.2. Identification of Optimum of Temperature and Pressure of Reaction

In order to identify the optimum temperature and pressure of the reaction and the effect of these two parameters of the reaction on the appearance of CaPs ceramics, we examined materials synthesized under the following permanent conditions: reaction time of 5 h, Ca^{2+} ion concentration of 0.05 mol/dm^3, and stirring rate 250 rpm. The variable parameters were temperatures of 110 °C, 130 °C, 150 °C, 170 °C, and 200 °C with corresponding pressures of 20 bar, 2 bar, 4 bar, 6 bar, and 10 bar, respectively

The results for the materials obtained at the above conditions are presented in Table 4; SEM images are shown in Figure 7.

Table 4. The parameters of the CaPs ceramics obtained during hydrothermal synthesis at different temperatures and pressure (reaction conditions: Ca^{2+} 0.05 mol/dm^3, reaction time 5 h, 250 rpm, and reaction heating rate 2.5 °C/min).

Temperature (°C)	Pressure (bar)	Length (μm)	Width (μm)	Phase Composition (Form)
200	20	5.45–45.45	0.45–2.27	HAp (whiskers)
170	10	5.45–33.33	0.45–1.82	HAp (whiskers)
150	6	5.45–53.33	0.45–1.82	HAp (whiskers)
130	4	5.45–50.0	0.45–2.27	HAp (whiskers)
110	2	3.18–21.36	0.45–1.36	81.40% Monetite (plate formations), 18.60% HAp (whiskers)

The whiskers were obtained in all the syntheses, regardless of the temperature and pressure during the reaction (Figure 7a–d). The mean length of the whiskers ranged from 5.45 to 53.33 μm, except for particles fabricated at 110 °C (Figure 7e) where the length was of the smallest values ranging from 3.18 to 21.36 μm.

Figure 8 presents the XRD patterns for the obtained ceramic powders. The XRD analysis indicates that the main product of the synthesis conducted at the low temperature of 110 °C and pressure of 2 bars was monetite (triclinic and P1), 81.4%. In this case, the hydroxyapatite (hexagonal and P 63/m) appeared as a second phase in the amount of 18.6%. The increase in the temperature (above 130 °C) and the pressure (above 4 bar) led to products with a content of 100% hydroxyapatite (hexagonal and P 63/m). We have observed that all the diffraction peaks were narrower when increasing the synthesis temperature and pressure. This implies that the samples were of higher crystallinity and crystallite size. Moreover, the increase in the *a* and the *c* lattice structure parameters with temperature and pressure was observed (Table S2), which can indicate a formation of the carbonated HAp.
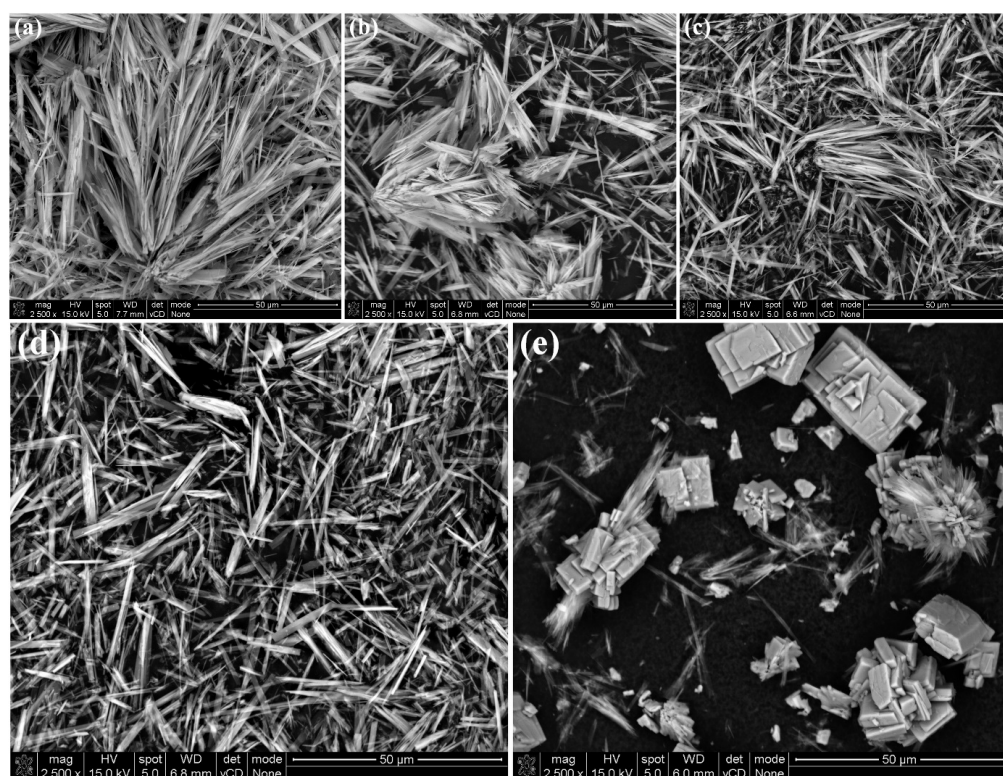
Figure 7. SEM images of products obtained in hydrothermal synthesis (reaction conditions: Ca^{2+} 0.05 mol/dm^3, 200 °C, 5 h, and 250 rpm): (**a**) 200 °C and 20 bar, (**b**) 170 °C and 10 bar, (**c**) 150 °C and 6 bar, (**d**) 130 °C and 4 bar, and (**e**) 110°C and 2 bar.(Magnification of 2500×.)
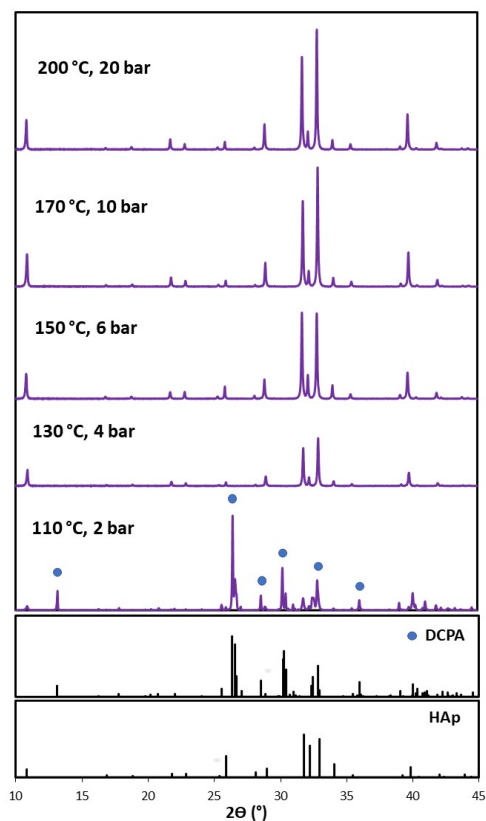

Figure 8. XRD patterns of powders obtained at different temperature and pressure (reaction conditions: Ca^{2+} 0.05 mol/dm^3, 200°C, 5 h, and 250 rpm).

Based on the obtained results, it is possible to identify the optimum temperature and pressure of the reaction for obtaining pure HAp, which was a temperature of 200 °C and a pressure of 20 bar. We have observed that the efficiency of the reaction increases with increasing temperature.

3.3. Identification of the Optimum Stirring Rate during the Reactions

After investigation on the optimum stirring rate during the reaction, the effect of this parameter on the character of calcium phosphates ceramics was determined. The stirring rate during hydrothermal synthesis, i.e., the main factor controlling the area of reagent's contact, obviously should have a significant impact on HAp morphology. The effect of the stirring rate on the phase composition and morphology of prepared products was determined for materials obtained at the following conditions: Ca^{2+} 0.05 mol/dm^3, reaction time 5 h, reaction temperature of 200 °C, pressure of 20 bar, and variable stirring rates of 0 rpm, 62.5 rpm, 125 rpm, 250 rpm, 750 rpm, and 1000 rpm. Reaction parameters, morphology, and phase composition results are presented in Table 5.

Table 5. The parameters of the CaPs ceramics obtained during hydrothermal synthesis at different stirring rates (reaction conditions: Ca^{2+} 0.05 mol/dm^3, reaction time 5 h, 200 °C, pressure 20 bar, and reaction heating rate 2.5 °C/min).

Stirring Rate (rpm)	Length (μm)	Width (μm)	Phase Composition (Form)
0	6.66–44.44	0.22–1.11	HAp (whiskers, flowers, chrysanthemums)
62.5	4.89–54.54	0.22–1.11	HAp (whiskers, flowers, chrysanthemums)
125	4.09–50.0	0.45–2.72	HAp (whiskers)
250	11.78–43.18	0.22–2	HAp (whiskers)
500	5.91–66.67	0.45–3.33	HAp (whiskers, flowers, cylinders)
750	5.45–27.27	0.45–2.72	HAp (whiskers)
1000	5.45–27.77	0.45–1.82	HAp (whiskers, flowers, cylinders)

The products' morphologies are shown in Figure 9. During the reaction without stirring (Figure 9a), HAp is represented by three morphological forms: whiskers (6.66–44.44 μm), flowers, and particles similar to chrysanthemums. The same was observed for the process with slow mixing (stirring rate of 62.5 rpm), which led to the formation of whiskers (4.89–54.54 μm), flowers, and chrysanthemums (Figure 9b).

The most homogeneous product in the form of the whiskers was obtained for higher stirring rates of 125 rpm (4.09–50.0 μm) (Figure 9c), 250 rpm (11.78–43.18 μm) (Figure 9d), and 750 rpm (5.45–27.27) μm) (Figure 9e). As expected, too high stirring rate will mainly affect the length of the particles, and this was proven for the products obtained at a stirring rate of 1000 rpm, which presented as short whiskers (5.45–27.77 μm). For this material, other particles also formed in the shape of flowers and cylinders (Figure 9f).

The XRD patterns obtained for the powders are presented in Figure 10. The lattice parameters of the present phases are included in Table S3. The XRD analysis showed that the stirring rate did not affect the phase composition of synthesized powders. All the obtained XRD patterns were characteristic of hydroxyapatite (hexagonal and P 63/m), and no impurities were detected. What can be clearly seen is that the shape of the peaks was nearly the same, and their high intensities indicate a high degree of crystallinity. Almost all the synthesized powders (except of materials obtained at a stirring rate of 1000 rpm) had a strong tendency for orientation, which is demonstrated by the increased intensity of the (300) peak at 2θ = 32.9°. When the stirring rate increases, the *a* and *c* parameters decrease. Additionally, the cell volume of obtained hydroxyapatites also decreases.
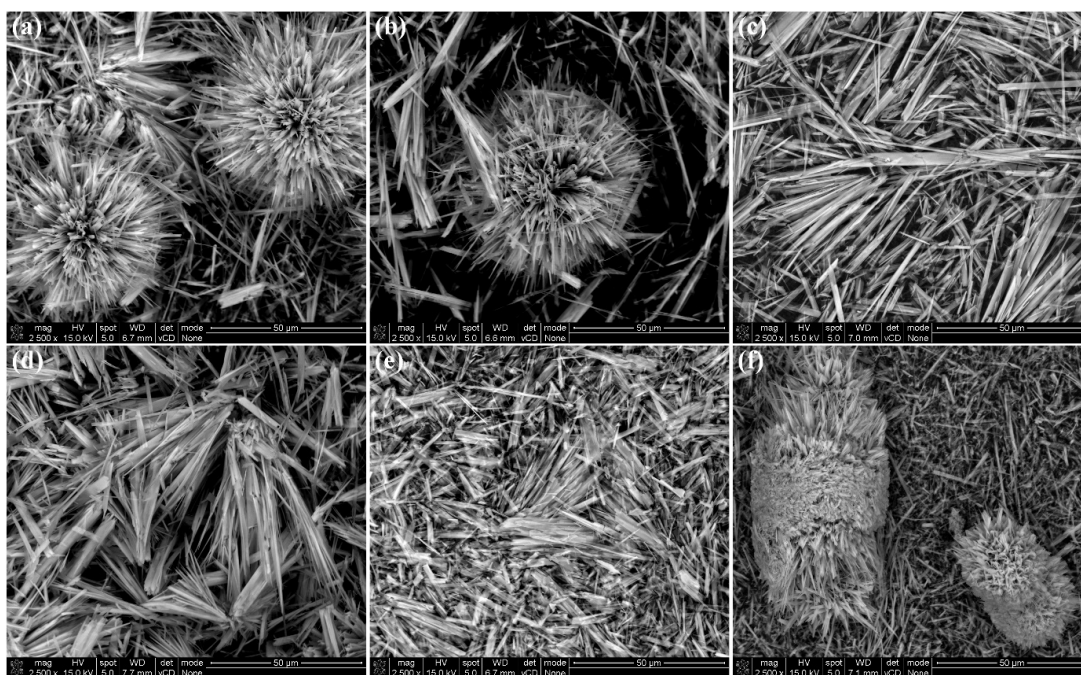
Figure 9. SEM images of products obtained in hydrothermal synthesis (200 °C, 20 bar, 5 h, and Ca^{2+} 0.05 mol/dm^3) at stirring rates (rpm): (**a**) 0, (**b**) 62.5, (**c**) 125, (**d**) 250, (**e**) 750, and (**f**) 1000 rpm (magnification of 2500×).
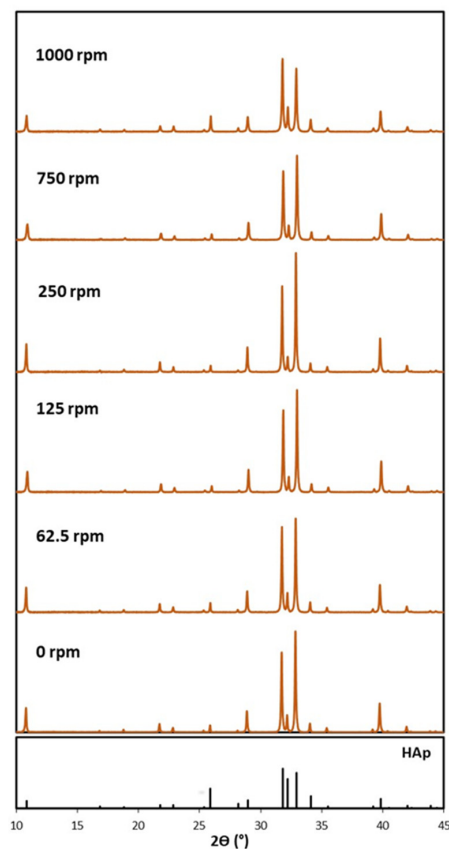

Figure 10. XRD patterns of powders obtained at different stirring rates (reaction conditions: 200 °C, 20 bar, 5 h, and Ca^{2+} 0.05 mol/dm^3).

Based on the obtained results, the optimum stirring rates for the reaction can be identified. The most homogeneous product in the form of the HAp whiskers, without any agglomerates, can be obtained with a stirring rate of 250 rpm.

3.4. Identification of Optimum pH of Mixture Reaction

In this paper, we also investigate the influence of pH of the reaction mixture on the appearance and crystallinity of ceramics. Thus, we chose the following permanent reaction conditions to be tested: Ca^{2+} 0.05 mol/dm^3, reaction time of 5 h, temperature of 200 °C, and stirring rate 250 rpm. For the materials obtained under this procedure, we performed only morphological (SEM) and structural (XRD) characterization.

The results for the examination of the relationship of CaPs ceramic's phase composition and shape to the pH with the starting reaction solution are presented in Table 6, and the SEM images of the obtained HAp are shown in Figure 11.

Table 6. The parameters of the ceramics obtained during hydrothermal synthesis at different pH (reaction conditions: Ca^{2+} 0.05 mol/dm^3, reaction time 5 h, 200 °C, pressure 20 bar, 250 rpm, and reaction heating rate 2.5 °C/min).

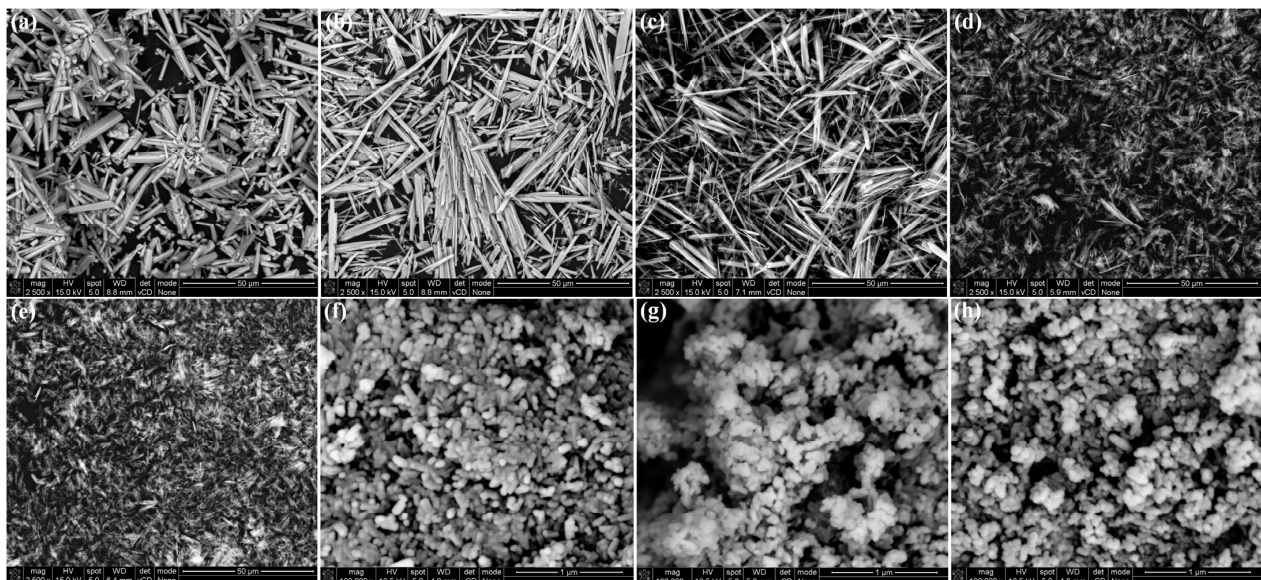| pH	Length (μm)	Width (μm)	Phase Composition (Form)
3.48	8.89–40.91	0.91–2.27	HAp (hexagonal rods)
4.0	18.88–77.77	0.91–2.72	HAp (whiskers)
4.52	3.33–26.66	0.44–1.11	HAp (whiskers)
4.75	18.6 -53.64	0.44–1.77	HAp (whiskers)
4.83	4.09–13.64	0.91–1.82	HAp (whiskers)
5.06	2.22–9.10	0.22–0.91	HAp (whiskers)
5.57	94.44–138.89 nm	34.6–49.8 nm	HAp (nano)
9.02	50.0–93.75 nm	37.1–55.8 nm	HAp (nano)
11.01	41.7–88.89 nm	41.7–50.0 nm	HAp (nano)

Figure 11. SEM images of HAp obtained using hydrothermal synthesis (Ca^{2+} 0.05 mol/dm^3, 200 °C, and 20 bar): (**a**) pH 3.48, (**b**) pH 4.04, (**c**) pH 4.52, (**d**) pH 4.83, (**e**) pH 5.06, (**f**) pH 5.57, (**g**) pH 9.02, and (**h**) pH 11.01. (**a**–**e**) Magnification of 2500× and (**f**–**h**) magnification of 100,000×).

Figure 11 shows the SEM microphotographs obtained for different pH conditions. For most products, the SEM images were taken at 2500× magnification, while in the case of nano-HAp, the magnification was 100.000×. The purpose this comparison was to

present the possibility of obtaining HAp with different morphologies under the proposed reaction conditions.

The hexagonal rods (8.89–40.91 µm) were obtained only for the product synthesized from starting solutions with a pH of 3.48 (Figure 11a). The whiskers were identified in material prepared at pH ranging from 4.04 to 5.06 (Figure 11b–e), whereas the nano-HAp was produced when the pH of the starting solution was kept in the range of 5.57–11.01 (Figure 11f–h). The general observation for this part of our research is that as the pH increases, the length of the whiskers decreases.

The XRD patterns of the obtained HAp are shown in Figure 12. The XRD analysis on this part of the ceramic material (reaction conditions: Ca^{2+} 0.05 mol/dm^3, 200 °C, 5 h, and 20 bar) revealed that regardless of the pH, the only phase presented in the samples was hydroxyapatite (hexagonal and P 63/m).
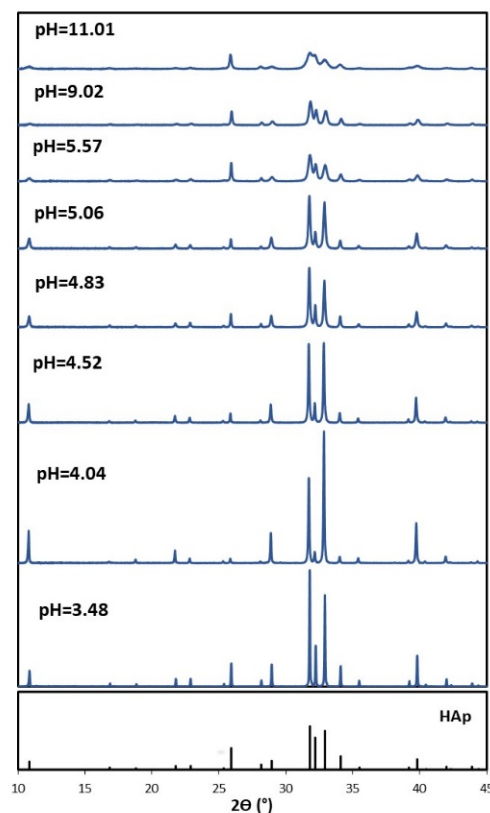

Figure 12. XRD patterns of powders obtained at different pH (reaction conditions: Ca^{2+} 0.05mol/dm^3, 200 °C, 5 h, and 20 bar).

It was noticed that the pH mostly affects the cell parameters and the crystallite size (Table 7)—with an increase in the pH, the cell volume decreases. Decreasing of the *a* and *c* parameters may indicate the formation of HAp without carbonate groups in the structure (*a* and *c* decreased). The lowering and widening of the peaks with increasing pH confirms the reduction in their crystallinity and grain size.

By changing the pH of the mixture reaction, it is possible to control the morphology of the resulting hydroxyapatite. Based on the obtained test results, it is possible to identify the optimal pH of a mixture reaction for obtaining HAp in the form of hexagonal rods, which is pH = 3.48 (Ca^{2+} ion concentrations 0.05 mol/dm^3, temperature of 200 °C). In the pH range of a mixture reaction from 4.0 to 5.06 it is feasible to obtain HAp in the form of whiskers. Additionally, by increasing the pH, it is possible to influence the length of whiskers. The optimum pH for whiskers fabrication is about 4.5, because at this pH value, the cloudiness of the solution disappears due to the addition of a sufficient amount of nitric

acid. Finally, in the pH range of 5.57–11.01, nano-HAp can be obtained. A higher pH is more advantageous due to its higher reaction efficiency.

Table 7. Effects of the pH on the lattice parameters of the identified phases (reaction conditions: Ca^{2+} 0.05 mol/dm^3, 200 °C, 5 h, 250 rpm, and 20 bar).

pH	Phase Composition	COD	Crystal Lattice Parameters		
			$a = b$ (Å)	c (Å)	V * (Å^3)
11.01	HAp	9001233 [48]	9.41660	6.87450	527.91
9.02	HAp	9001233 [48]	9.41660	6.87450	527.91
5.57	HAp	9001233 [48]	9.41660	6.87450	527.91
5.06	HAp	9011092 [49]	9.42400	6.87900	529.09
4.83	HAp	9011092 [49]	9.42400	6.87900	529.09
4.52	HAp	9002214 [50]	9.43940	6.88610	531.36
4.04	HAp	9002214 [50]	9.43940	6.88610	531.36
3.48	HAp	9002214 [50]	9.43940	6.88610	531.36

* cell volume.

4. Discussion

Our goal in this study was to investigate the influence of synthesis conditions on the properties of calcium phosphates ceramics. It was already proven that the hydrothermal process parameters, such as the concentration of the calcium precursor, can have a significant impact on the crystallite size, specific surface area, phase composition, or crystal lattice parameters of apatite ceramics [58,59].

The potential application of hydroxyapatite and other apatites is strongly dependent on their morphology. We observed that this feature was the most affected by the process parameters, and we will focus on its variation at first. Andrés-Vergés et al. [59] noticed that hydrothermal decomposition of calcium chelate can be used to synthesize needle crystals of HAp, while the temperature and pH of the reaction mixture influence both the diameter and length of the resulting HAp crystals. According to Table 1, the concentrations of Ca^{2+} ions influence the morphology of the obtained HAp in two ways. At low Ca^{2+} concentrations of 0.025–0.05 mol/dm^3, a small number of nuclei are formed, which results in slower crystallization and the formation of elongated whiskers in the range of crystal lattice parameters of $a = b$ 9.41660–9.42400 (Å), c 6.87450–6.87900 (Å), and 527.91–529.09 V (Å3). On the other hand, at higher calcium ion concentrations of 0.1–0.2 mol/dm^3, a large number of nuclei formed resulting in faster crystallization and the formation of numerous short hexagonal rods with the crystal lattice parameters of $a = b$ 9.42400–9.43940 (Å), c 6.87900–6.88610 (Å), and 529.09–531.36 V(Å^3). Similar observations were presented by Roeder et al. [43], who investigated the formation of HAp whiskers by changing the heating rate, stirring rate, and reaction temperature; therefore, the parameters mostly affected the release rate of the calcium ions. Our results also showed that as the Ca^{2+} concentration increases, the length of HAp particles decreases, which is in line with previous studies.

Additionally, the pH of the solution has a pronounced influence on the morphology of the obtained CaPs, as is shown in Table 7, where the results of the morphological investigation with varied pHs were presented. We observed that at an initial pH of about 3.48 it was possible to obtain pure HAp in shape of hexagonal rods. As the pH increases to the values in the range of 4.0–5.06, the shape of HAp changes and whiskers are formed. A further increase in pH (pH = 5.57–11.01) results in a reduction in particle size and formation of nano-HAp with crystal lattice parameters of $a = b$ 9.41660 (Å), c 6.87450 (Å), and 527.91 V (Å^3).

By analyzing the rest of the process conditions, i.e., reaction time and temperature, we observed that they do not affect the morphology of apatite ceramics; however, it should be emphasized that reaction time is linked with the Ca^{2+} concentration. The correlation of these two parameters will result in different HAp morphologies. Regarding the phase composition, we have observed no influence of the reaction time or Ca^{2+} concentration on the phase composition of the obtained ceramics, in contrast to changing the synthesis temperature. Each reaction led to pure hydroxyapatite, regardless of the reagent concentrations and reaction times. The only exception was the process performed for 1 h and at 0.2 Ca^{2+}, which resulted in a mixture of HAp (hexagonal rods) and monetite (plate formations). This is probably because too high Ca^{2+} concentration and too short reaction time are the parameters that hinder HAp crystal formation. It is likely that monetite crystals require less energy (lower temperature) and a shorter time to be formed. Moreover, for temperatures above 130 °C pure HAp was identified, while for the synthesis conducted at 110 °C, HAp was in the minority (18.60%) and the monetite represents the major phase at 81.40%. This is another proof that less stable monetite also require less energy for crystallization compared to hydroxyapatite.

Infrared structural investigation of the obtained ceramics demonstrated that the materials showed almost all the characteristic bands for hydroxyapatite. It should be noted that the shape of the most prominent band on the IR spectra, which is the one observed at around 1031 cm^{-1} related to $PO_4{}^{3-}$, differs for the materials depending on the Ca^{2+} concentration and reaction time. For those with concentrations higher than 0.10 mL/dm^3 of Ca^{2+} ions, the band is separated into two at 1023 cm^{-1} and 1047 cm^{-1}, which is the sign that the surrounding of $PO_4{}^{3-}$ is different as well. The presence of medium bands in the range of 872–878 cm^{-1}, which are assigned to ν_3 C-O ($CO_3{}^{2-}$) vibrations, is a singular proof of the carbonate ion's presence in the synthesized HAp.

When analyzing the XRD data, we noticed that while increasing the Ca^{2+} concentration a slight shift of diffraction peaks to the left side can be observed, which is a consequence of the increase in the *a* and the *c* crystal lattice parameters and phase cell volume (Table 2). The possible explanation is that the incorporation of carbonate groups in the place of hydroxyl or/and phosphate groups led to a change in the *a* and *c* parameters [60]. As was previously reported, the XRD patterns for hydroxyapatite particles displayed a stronger preference for (300) reflection (2θ = 32.9°), which become stronger with the growth of the crystallite's sizes. Moreover, hydroxyapatite crystals may be grown in different directions under hydrothermal reaction conditions, which is equal to their anisotropy, and has also previously been observed by others [39].

An important feature of the fillers is the specific surface area (S_{BET}), which is also strongly related to the possibility of further modification and resorption ability. Our results showed that the specific surface area of apatite ceramics changed with the concentration of Ca^{2+} ions and resulting from the different ceramics' morphologies. S_{BET} decreased with an increasing concentration of Ca^{2+}; a low Ca^{2+} concentration of 0.05 mol/dm^3 led to an S_{BET} of 6.6538 ± 0.0503 m^2/g (whiskers), while the highest of the tested Ca^{2+} concentrations (0.2 mol/dm^3) reduced S_{BET} to the value of 0.9310 ± 0.0146 m^2/g (hexagonal rods), whereas for nanorods obtained at Ca^{2+} = 0.05 mol/dm^3, the S_{BET} was 71.3623 ± 0.2185 m^2/g, which is more or less obvious considering the size of HAp particles.

A very important process parameter, the stirring rate, was found to strongly affect the morphology of CaP ceramics. The most homogeneous product in the form of the HAp whiskers was obtained at higher stirring rates of 125 rpm and 250 rpm, while lower or higher stirring rates resulted in the mixtures different morphological forms. This is an obvious effect of different environments for crystals formation—insufficient contact area at a low stirring rate (the same environment) or a higher stirring rate (short time of reagent's contact) will yield various crystal forms.

Our results proved that the HAp morphology can be easily controlled by changing the Ca^{2+} ion concentration, pH, the reaction temperature, and the stirring rate. In this way, it is possible to obtain hydroxyapatite of different morphologies such as whiskers,

hexagonal rods, nano-HAp, and more complex forms (e.g., flowers and chrysanthemums). After careful evaluation and comparison of all the results we can propose the following range of parameters for obtaining whiskers: concentrations of Ca^{2+} ions in the range of 0.025–0.05 mol/dm^3, reaction time of 5h, pH in the range of 4.0–5.06, temperature of 200 °C, and pressure of 20bar. In the case of other morphological forms of HAp, the permanent parameters are the reaction time of 5 h, reaction temperature of 200 °C, and pressure of 20 bars. Therefore, when keeping the above conditions, hexagonal rods are possible to prepare at concentrations of Ca^{2+} ions in the range of 0.1–0.2 mol/dm^3 and pH at a low level of not more than 3.5. When nano-sized HAp particles are desired, it is necessary to keep the Ca^{2+} concentration at the low level of 0.05 mol/dm^3 and pH in the range of 9–11.

A general conclusion is that comparing to the procedure with orthophosphoric acid as a phosphorous precursor, the reaction reported here, with dipotassium hydrogen phosphate, is more effective for controlling the ceramics' characteristics [44]. We can also conclude that Ca^{2+} concentration is one of the most important parameters to be considered, regardless of the reaction type. Regarding the temperature of the process, in previous study [44,45] only a high temperature of 200 °C led to HAp whiskers, in contrast to the results reported here, which is another proof that this procedure allows for controlling ceramics' appearance and phase composition.

5. Conclusions

In this paper, hydroxyapatite was successfully prepared in the reaction between calcium lactate pentahydrate and dipotassium hydrogen phosphate. HAp whiskers, hexagonal rods, and nano particles were obtained under the hydrothermal method. The advantage of the proposed method is the facile but accurate control of the HAp crystal morphology in order to produce materials in a desired form, which could be potentially used in the biomedical field.

The effect of reagent concentrations, reaction time, pH, temperature, pressure, and stirring rate on HAp morphologies and composition was investigated. The results of the study showed that the main influences on the morphology are the concentration of Ca^{2+} and pH. Parameters such as temperature, stirring rate, and pressure have lower impact on ceramics morphology.

The measurements showed that the optimal reaction parameters for obtaining whiskers are Ca^{2+} 0.05 mol/dm^3, reaction time 5 h, reaction temperature of 200 °C, pressure of 20 bar, stirring rate of 250 rpm, and pH = 4.5. For hexagonal rods the optimal parameters are Ca^{2+} 0.2 mol/dm^3, 5 h, 200 °C, 20 bar, 250 rpm, pH = 4.5. For nano HAp the optimal parameters are Ca^{2+} 0.2 mol/dm^3, 5 h, 200 °C, 20 bar, 250 rpm, and pH = 11.0.

This investigation can have a great impact in the development of biomaterials for orthopedic applications. Our optimized method results in hydroxyapatite of different forms such as whiskers, hexagonal rods, and nanoparticles that can be used as functional fillers in composites for medical applications.

Author Contributions: P.S.: conceptualization, methodology, design, preparation of synthesis, analysis and interpretation of data, manuscript writing, and corrections A.A.: investigation (X-ray diffraction and BET) and analysis and interpretation of data, J.P.: investigation (FTIR), analysis and interpretation of data, manuscript writing, and corrections, P.T.-G.: investigation (SEM, STEM, and observations). All authors have read and agreed to the published version of the manuscript.

References

1. Samavedi, S.; Whittington, A.R.; Goldstein, A.S. Calcium phosphate ceramics in bone tissue engineering: A review of properties and their influence on cell behavior. *Acta Biomater.* **2013**, *9*, 8037–8045. [CrossRef] [PubMed]
2. Habraken, W.; Habibovic, P.; Epple, A.; Bohner, M. Calcium phosphates in biomedical applications: Materials for the future? *Mater. Today* **2016**, *19*, 69–87. [CrossRef]
3. Canillas, M.; Pena, P.; de Aza, A.H.; Rodríguez, M.A. Calcium phosphates for biomedical applications. *Boletín De La Soc. Española De Cerámica Y Vidr.* **2017**, *56*, 91–112. [CrossRef]
4. Dorozhkin, S.V. Calcium orthophosphate bioceramics. *Ceram. Int.* **2015**, *41*, 3913–3966. [CrossRef]
5. Kattimani, V.S.; Kondaka, S.; Lingamaneni, K.P. Hydroxyapatite—Past, Present, and Future in Bone Regene. *Bone Tissue Regen. Insights* **2016**, *7*, 9–19. [CrossRef]
6. Šupová, M. Substituted hydroxyapatites for biomedical applications: A review. *Ceram. Int.* **2015**, *41*, 9203–9231. [CrossRef]
7. Roeder, R.K.; Sproul, M.S.; Turner, C.H. Hydroxyapatite Whiskers Provide Improved Mechanical Properties in Reinforced Polymer Composites. *J. Biomed. Mater. Res.* **2003**, *67*, 801–812. [CrossRef]
8. Milazzo, M.; Contessi Negrini, N.C.; Scialla, S.; Marelli, B.; Farè, S.; Danti, S.; Buehler, M.J. Additive Manufacturing Approaches for Hydroxyapatite-Reinforced Composites. *Adv. Funct. Mater.* **2019**, *29*, 1903055. [CrossRef]
9. Tasdemir, M.; Kenet, I.H.; Pazarlioglu, S. Hydroxyapatite reinforced polypropylene bio composites. *Acad. J. Sci.* **2016**, *6*, 461–468.
10. Bohara, S.; Suthakorn, J. Surface coating of orthopedic implant to enhance the osseointegration and reduction of bacterial colonization: A review. *Biomater. Res.* **2022**, *26*, 26. [CrossRef]
11. Meyer, F.; Amaechi, B.T.; Fabritius, H.O.; Enax, J. Overview of Calcium Phosphates used in Biomimetic Oral Care. *Open Dent. J.* **2018**, *12*, 406–423. [CrossRef] [PubMed]
12. Dorozhkin, S.V. Calcium orthophosphates in dentistry. *J. Mater. Sci. Mater. Med.* **2013**, *24*, 1335–1363. [CrossRef] [PubMed]
13. Balhuc, S.; Campian, R.; Labunet, A.; Negucioiu, M.; Buduru, S.; Kui, A. Dental Applications of Systems Based on Hydroxyapatite Nanoparticles—An Evidence-Based Update. *Crystals* **2021**, *11*, 674. [CrossRef]
14. Izzetti, R.; Gennai, S.; Nisi, M.; Gulia, F.; Miceli, M.; Giuca, M.R. Clinical Applications of Nano-Hydroxyapatite in Dentistry. *Appl. Sci.* **2022**, *12*, 10762. [CrossRef]
15. Carella, F.; Esposti, L.D.; Adamiano, A.; Iafisco, M. The Use of Calcium Phosphates in Cosmetics, State of the Art and Future Perspectives. *Materials* **2021**, *14*, 6398. [CrossRef]
16. Lara-Ochoa, S.; Ortega-Lara, W.; Guerrero-Beltrán, C.E. Hydroxyapatite Nanoparticles in Drug Delivery: Physicochemistry and Applications. *Pharmaceutics* **2021**, *13*, 1642. [CrossRef]
17. Wen, Y.; Li, J.; Lin, H.; Huang, H.; Song, K.; Duan, K.; Guo, T.; Weng, J. Improvement of Drug-Loading Properties of Hydroxyapatite Particles Using Triethylamine as a Capping Agent: A Novel Approach. *Crystals* **2021**, *11*, 703. [CrossRef]
18. Marincaș, L.; Turdean, G.L.; Toșa, M.; Kovács, Z.; Kovács, B.; Barabás, R.; Farkas, N.-I.; Bizo, L. Hydroxyapatite and Silicon-Modified Hydroxyapatite as Drug Carriers for 4-Aminopyridine. *Crystals* **2021**, *11*, 1124. [CrossRef]
19. Kolmas, J.; Krukowski, S.; Laskus, A.; Jurkitewicz, M. Synthetic hydroxyapatite in pharmaceutical applications. *Ceram. Int.* **2016**, *42*, 2472–2487. [CrossRef]
20. Cummings, L.J.; Snyder, M.A.; Brisack, K. Protein chromatography on hydroxyapatite columns. *Methods Enzymol.* **2009**, *463*, 387–404. [CrossRef]
21. Fihri, A.; Len, C.; Varma, R.S.; Solhy, A. Hydroxyapatite: A review of syntheses, structure and applications in heterogeneous catalysis. *Coord. Chem. Rev.* **2017**, *347*, 48–76. [CrossRef]
22. Nayak, A.; Bhushan, B. Hydroxyapatite as an advanced adsorbent for removal of heavy metal ions from water: Focus on its applications and limitations. *Mater. Today Proc.* **2021**, *46*, 11029–11034. [CrossRef]
23. Ibrahim, M.; Labaki, M.; Giraudon, J.-M.; Lamonier, J.-F. Hydroxyapatite, a multifunctional material for air, water and soil pollution control: A review. *J. Hazard. Mater.* **2020**, *383*, 121139. [CrossRef] [PubMed]
24. Nasr-Esfahani, M.; Fekri, S. Alumina/TiO$_2$/hydroxyapatite interface nanostructure composite filters as efficient photocatalysts for the purification of air. *Reac. Kinet. Mech. Catal.* **2012**, *107*, 89–103. [CrossRef]

25. Baldassarre, F.; Altomare, A.; Mesto, E.; Lacalamita, M.; Dida, B.; Mele, A.; Bauer, E.M.; Puzone, M.; Tempesta, E.; Capelli, D.; et al. Structural Characterization of Low-Sr-Doped Hydroxyapatite Obtained by Solid-State Synthesis. *Crystals* **2023**, *13*, 117. [CrossRef]

26. Pu'ad, N.A.S.M.; Haq, R.H.A.; Noh, H.M.; Abdullah, H.Z.; Idris, M.; Chuan, L.T. Synthesis method of hydroxyapatite: A review. *Mater. Today Proc.* **2020**, *29*, 233–239. [CrossRef]

27. Abidi, S.S.A.; Murtaza, Q. Synthesis and Characterization of Nano-hydroxyapatite Powder Using Wet, Chemical Precipitation Reaction. *J. Mater. Sci. Technol.* **2014**, *30*, 307–310. [CrossRef]

28. Espanol, M.; Portillo, J.; Manero, J.M.; Ginebra, M.P. Investigation of the hydroxyapatite obtained as hydrolysis product of α-tricalcium phosphate by transmission electron microscopy. *Cryst. Eng. Comm.* **2010**, *12*, 3318–3326. [CrossRef]

29. Agrawal, K.; Singh, G.; Puri, D.; Prakash, S. Synthesis and Characterization of Hydroxyapatite Powder by Sol-Gel Method for Biomedical Application. *J. Miner. Mater. Charact. Eng.* **2011**, *10*, 727–734. [CrossRef]

30. Yang, Y.; Wu, Q.W.; Wang, M.; Long, J.; Mao, Z.; Chen, X. Hydrothermal Synthesis of Hydroxyapatite with Different Morphologies: Influence of Supersaturation of the Reaction System. *Cryst. Growth Des.* **2014**, *14*, 4864–4871. [CrossRef]

31. Noviyanti, A.R.; Asyiah, E.N.; Permana, M.D.; Dwiyanti, D.; Suryana; Eddy, D.R. Preparation of Hydroxyapatite-Titanium Dioxide Composite from Eggshell by Hydrothermal Method: Characterization and Antibacterial Activity. *Crystals* **2022**, *12*, 1599. [CrossRef]

32. Jarudilokkul, S.; Tanthapanichakoon, W.; Boonamnuayvittaya, V. Synthesis of hydroxyapatite nanoparticles using an emulsion liquid membrane system. *Colloids Surf. A Physicochem. Eng. Asp.* **2007**, *296*, 149–153. [CrossRef]

33. Yoruç, A.B.H.; İpek, Y. Sonochemical Synthesis of Hydroxyapatite Nanoparticles with Different Precursor Reagents. *Acta Phys. Pol. A* **2012**, *121*, 230–232. [CrossRef]

34. Sánchez-Hernández, A.K.; Martínez-Juárez, J.; Gervacio-Arciniega, J.J.; Silva-González, R.; Robles-Águila, M.J. Effect of Ultra-sound Irradiation on the Synthesis of Hydroxyapatite/Titanium Oxide Nanocomposites. *Crystals.* **2020**, *10*, 959. [CrossRef]

35. Ruffini, A.; Sprio, S.; Preti, L.; Tampieri, A. Synthesis of Nanostructured Hydroxyapatite via Controlled Hydrothermal Route. In *Biomaterial-Supported Tissue Reconstruction or Regeneration*; Barbeck, M., Jung, O., Smeets, R., Koržinskas, T., Eds.; IntechOpen: London, UK, 2019. [CrossRef]

36. Liu, J.; Ye, X.; Wang, H.; Zhu, M.; Wang, B.; Yan, H. The influence of pH and temperature on the morphology of hydroxyapatite synthesized by hydrothermal method. *Ceram. Int.* **2003**, *29*, 629–633. [CrossRef]

37. Ebrahimi, S.; Sipaut, S.; Mohd Nasri, C.; Bin Arshad, S.E. Hydrothermal synthesis of hydroxyapatite powders using Response Surface. Methodology (RSM). *PLoS ONE* **2001**, *16*, e0251009. [CrossRef]

38. Ortiz, L.S.; Anaya, D.M.; Sánchez-Campos, D.; Fernandez-García, M.E.; Salinas, E.; Reyes-Valderrama, M.I.; Rodriguez Lugo, V. The pH Effect on the Growth of Hexagonal and Monoclinic Hydroxyapatite Synthesized by the Hydrothermal Method. *J. Nanomater.* **2020**, *2*, 1–10. [CrossRef]

39. Suchanek, K.; Bartkowiak, A.; Perzanowski, M.; Marszałek, M. From monetite plate to hydroxyapatite nanofibers by mo-noethanolamine assisted hydrothermal approach. *Sci. Rep.* **2018**, *8*, 15408. [CrossRef]

40. Kati, N.; Ozan, S.; Yildiz, T.; Arslan, M. Effect of Reaction Time and Heat Treatment in the Production of Hydroxyapatite by Hydrothermal Synthesis. *Arch. Metall. Mater.* **2022**, *4*, 1427–1434. [CrossRef]

41. Kuśnieruk, S.; Wojnarowicz, J.; Chodara, A.; Chudoba, T.; Gierlotka, S.; Lojkowski, W. Influence of hydrothermal synthesis parameters on the properties of hydroxyapatite nanoparticles. *Beilstein J. Nanotechnol.* **2016**, *7*, 1586–1601. [CrossRef]

42. Zhang, H.; Darvell, B.W. Morphology and structural characteristics of hydroxyapatite whiskers: Effect of the initial Ca concentra-tion, Ca/P ratio and pH. *Acta Biomater.* **2011**, *7*, 2960–2968. [CrossRef] [PubMed]

43. Roeder, R.K.; Converse, G.L.; Leng, H.; Yue, W. Kinetic Effects on Hydroxyapatite Whiskers Synthesized by the Chelate Decomposition Method. *J. Am. Ceram. Soc.* **2006**, *89*, 2096–2104. [CrossRef]

44. Szterner, P.; Biernat, M. The Synthesis of Hydroxyapatite by Hydrothermal Process with Calcium Lactate Pentahydrate: The Effect of Reagent Concentrations, pH, Temperature, and Pressure. *Bioinorg. Chem. Appl.* **2022**, *2020*, 3481677. [CrossRef] [PubMed]

45. Szterner, P.; Biernat, M. Effect of reaction time, heating and stirring rate on the morphology of HAp obtained by hydrothermal synthesis. *J. Therm. Anal. Cal.* **2022**, *147*, 13059–13071. [CrossRef]

46. Fujishiro, Y.; Yabuki, H.; Kawamura, K.; Sato, T.; Okuwaki, A. Preparation of Needle-like Hydroxyapatite by Homogeneous Precipitation under Hydrothermal Conditions. *J. Chem. Technol. Biotechnol.* **1993**, *57*, 349–353. [CrossRef] [PubMed]

47. Neira, I.S.; Guitián, F.; Taniguchi, T.; Watanabe, T. Hydrothermal synthesis of hydroxyapatite whiskers with sharp faceted hexagonal morphology. *J. Mater. Sci.* **2008**, *43*, 2171–2178. [CrossRef]

48. Hughes, J.M.; Cameron, M.; Crowley, K.D. Structural variations in natural F, OH, and Cl apatites. Locality: Holly Springs, GA, USA. *Am. Mineral.* **1989**, *74*, 870–876.

49. Sudarsanan, K.; Young, R.A. Significant precision in crystal structural details: Holly Springs hydroxyapatite Locality: Holly Springs, Cherokee County, Georgia, USA Sample: X-23-6. *Acta Crystallogr. Sect. B* **1969**, *25*, 1534–1543. [CrossRef]

50. Wilson, R.M.; Elliot, J.C.; Dowker, S.E.P. Rietveld refinement of the crystallographic structure of human dental enamel apatites Sample: H6G. *Synth. Am. Mineral.* **1999**, *84*, 1406–1414. [CrossRef]

51. Catti, M.; Ferraris, G.; Filhol, A. Hydrogen bonding in the crystalline state. $CaHPO_4$ (monetite), P-1 or P1? A novel neutron diffraction study Locality. *Synth. Acta Crystallogr. Sect. B* **1977**, *33*, 1223–1229. [CrossRef]

52. Zakaria, F.Z.; Mihaly, J.; Sajo, I.; Katona, R.; Hajba, L.; Aziz, F.A.; Mink, J. FT-Raman and FTIR spectroscopic characterization of biogenic carbonates from Philippine venus seashell and Porites sp. coral. *J. Raman. Spectrosc.* **2008**, *39*, 1204–1209. [CrossRef]

53. Markowic, M.; Fowler, B.O.; Tung, M.S. Preparation and Comprehensive Characterization of a Calcium Xydroxyapatite Reference Material. *J. Res. Natl. Inst. Stand. Technol.* **2004**, *109*, 553–568. [CrossRef] [PubMed]

54. Bollino, F.; Armenia, E.; Tranquillo, E. Zirconia/Hydroxyapatite Composites Synthesized Via Sol-Gel: Influence of Hydroxyapatite Content and Heating on Their Biological Properties. *Materials* **2017**, *10*, 757. [CrossRef] [PubMed]

55. Yang, W.-G.; Ha, J.-H.; Kim, S.-G.; Chae, W.-S. Spectroscopic determination of alkyl resorcinol concentration in hydroxyapatite composite. *J. Anal. Sci. Technol.* **2016**, *7*, 9. [CrossRef]

56. Brunauer, S.; Emmett, P.H.; Teller, E. Adsorption of Gases in Multimolecular Layers. *J. Am. Chem. Soc.* **1938**, *60*, 309–319. [CrossRef]

57. Nasrollahzadeh, M.; Atarod, M.; Sajjadi, M.; Sajadi, S.M.; Issaabadi, Z. Chapter 6—Plant-Mediated Green Synthesis of Nanostructures: Mechanisms, Characterization, and Applications. *Interface Sci. Technol.* **2019**, *28*, 199–322. [CrossRef]

58. Xia, W.; Lin, K.; Gou, Z.; Engqvist, H. Morphology Control of HAp Crystals and its Aggregates Using ''Hard Templates'', Chapter VI. In *Hydroxyapatite: Synthesis, Properties and Applications*; Gshalaev, V.S., Demirchan, A.C., Eds.; Nova Science Publishers, Inc.: Hauppauge, NY, USA, 2012.

59. Andrés-Vergés, M.; Fernández-González, C.; Martínez-Gallego, M. Hydrothermal synthesis of calcium deficient hydroxyapatites with controlled size and homogeneous morphology. *J. Eur. Ceram. Soc.* **1998**, *18*, 1245–1250. [CrossRef]

60. Yang, W.H.; Xi, X.F.; Li, J.F.; Cai, K.Y. Comparison of Crystal Structure Between Carbonated Hydroxyapatite and Natural Bone Apatite with Theoretical Calculation. *Asian J. Chem.* **2013**, *25*, 3673–3678. [CrossRef]